crystals

MDPI

*Article*

# Controllable Functionalization of Carbon Dots as Selective and Sensitive Fluorescent Probes for Sensing Cu(II) Ions

**Xiaochun Zheng [1,*,†], Hao Zhang [2,†], Haoming Jiang [1], Lei Sun [1], Yuanze Sun [3], Qingcao Liu [2], Shoutian Ren [2,*], Yunpeng Zhuang [3] and Xiaofeng Gong [1]**

[1] Department of Intelligent Manufacturing, Yantai Vocational College, Yantai 264670, China; 13563138853@139.com (H.J.); 13940225803@163.com (L.S.); ytvcgxf@163.com (X.G.)
[2] Department of Optoelectronic Science, Harbin Institute of Technology at Weihai, Weihai 264209, China; 19862646374@163.com (H.Z.); qingcao.liu@hit.edu.cn (Q.L.)
[3] Department of Intelligent Control, Yantai Vocational College, Yantai 264670, China; 20240005@ytvc.edu.cn (Y.S.); yunpeng_zhuang@163.com (Y.Z.)
* Correspondence: 15053132811@163.com (X.Z.); renst77@163.com (S.R.)
† These authors contributed equally to this work.

**Abstract:** Carbon dots (CDs) are efficient fluorescent probes for metal ion detection due to their high sensitivity, nontoxicity and stability, but their rich functional groups lead to simultaneous responses to multiple ions. So, how to realize highly selective detection for specific ions is still a challenging task. In this work, "bare CDs" were synthesized using the electrochemical stripping method, followed by grafting with hydroxyl and carboxyl groups following the hydrothermal method with boric acid. Transmission electron microscopy, an X-ray diffractometer, Fourier transform infrared spectroscopy, UV–visible spectrophotometers and a fluorescence spectrometer were used to characterize their morphology, surface functional groups and optical properties, respectively. The modified CDs exhibit a high sensitivity of 65% and selectivity towards $Cu^{2+}$. Meanwhile, they also exhibited a short response time of less than 1 min and a good stability in terms of pH and ionic strength.

**Keywords:** fluorescent sensors; copper ion detection; functionalization; functional groups; quenching mechanism

check for updates

Academic Editor: Nabeen K Shrestha

Received: 21 January 2025
Revised: 11 February 2025
Accepted: 17 February 2025
Published: 21 February 2025

**Citation:** Zheng, X.; Zhang, H.; Jiang, H.; Sun, L.; Sun, Y.; Liu, Q.; Ren, S.; Zhuang, Y.; Gong, X. Controllable Functionalization of Carbon Dots as Selective and Sensitive Fluorescent Probes for Sensing Cu(II) Ions. *Crystals* **2025**, *15*, 205. https://doi.org/10.3390/cryst15030205

**Copyright:** © 2025 by the authors. Licensee MDPI, Basel, Switzerland. This article is an open access article distributed under the terms and conditions of the Creative Commons Attribution (CC BY) license (https://creativecommons.org/licenses/by/4.0/).

## 1. Introduction

In recent years, heavy metal pollution has brought a series of ecological and social problems, and cupric ion ($Cu^{2+}$) pollution is particularly noteworthy due to its wide application in electroplating, metallurgy and so on [1,2]. The safety threshold of $Cu^{2+}$ in drinking water was set to 20 ppm by the US Environmental Protection Agency [3]. Therefore, it is of great practical significance to develop a highly sensitive and selective method for $Cu^{2+}$ detection. Metal ions can easily react with fluorescent agents, which leads to fluorescence quenching, so the fluorescence quenching method is regarded as a perfect solution for metal ion detection, considering its high efficiency, low cost, simple operation and so on [4–6]. Among the various fluorescent agents, carbon dots (CDs) are considered as potential fluorescent probes due to their good fluorescence efficiency, excellent water solubility, good biocompatibility and low cost [7–10].

Since CDs were firstly synthesized as fluorescent probes for $Cu^{2+}$ detection in 2012 [11], abundant CD probes were successfully synthesized using multiple methods, such as hydrothermal [12], pyrolytic [13], the combustion/microwave-assisted method [14–17] and so on. These synthesized CDs are usually decorated with rich functional groups, such as

amino, carbonyl and carboxyl groups, leading to their simultaneous response to multiple ions and corresponding poor selectivity for specific ions [18]. Nowadays, some methods, such as the use of masking agents, heteroatom doping and post-processing, have been used to enhance the selectivity of CDs [10,19,20]. Post-processing is labor-intensive, but it is effective and has a low cost [21]. To achieve CD modification with specific functional groups, "bare CDs" with weak fluorescent signals are a superior alterative due to more easily grafting to specific functional groups. So, in this paper, "bare CDs" were first synthesized using the simple electrochemical stripping method and then modified by boric acid in a hydrothermal process to facilitate highly selective $Cu^{2+}$ detection.

## 2. Experimental Section

### *2.1. Materials*

All chemicals of analytical reagent grade were sourced from Aladdin Industrial Co., Shanghai, China, including $HgCl_2$, $K_2Cr_2O_7$, $AlCl_3{\cdot}6H_2O$, $LiOH{\cdot}6H_2O$, $Fe(NO_3)_3{\cdot}9H_2O$, $Mg(OH)_2$, $Mn(CH_3COO)_2$, $Sb(CH_3COO)_3$, $3CdSO_4{\cdot}6H_2O$, $CuSO_4{\cdot}5H_2O$, $ZnSO_4{\cdot}7H_2O$, $KNO_3$, $H_3BO_3$, quinine sulfate, $Na_2HPO_4$ and $KH_2PO_4$. Carbon rods of 4 mm in diameter were collected from a commercial battery, and throughout the entire experimental process, deionized water was used.

### *2.2. Synthesis of CDs*

Carbon nanosheets (CNs) were produced using the electrochemical stripping method outlined in a previous study [22]. In the standard procedure, two clean carbon rods were positioned parallel to each other, 7.5 cm apart, in 500 mL of deionized water, serving as the cathode and anode, respectively. A static potential of 15–60 V was applied between the electrodes using a direct current power supply. Following 120 h of electrochemical stripping, the solution transitioned from colorless to dark yellow, indicating the successful removal of CNs from the carbon electrode. The CN solution was then obtained by filtering through 0.22 μm filter paper and using a centrifuge at 22,000 rpm for 30 min.

Then, the hydrothermal method was used to selectively modify the CDs with hydroxyl and carboxyl functional groups. Following the typical procedure, 0.8 g of $H_3BO_3$ was thoroughly dissolved into 40 mL of CN solution, and the mixed solution was heated in a 50 mL autoclave at 180 °C for 6 h. After natural cooling to room temperature, the obtained solution was neutralized with 1 M NaOH solution and collected by centrifugation at 10,000 rpm for 30 min to obtain CDs, and these modified CDs were marked as bf-CDs. To clear unreacted salts, the bf-CDs were completely washed with ethanol and DI water, and then dried in a vacuum oven overnight.

### *2.3. Characterization*

The morphologies and lattice structure of the as-synthesized CDs were analyzed using transmission electron microscopy (TEM, JEOL, JEM-2100, Tokyo, Japan) and an X-ray diffractometer (XRD, Dandong Haoyuan, DX-2700, Dandong, China) equipped with Cu kα radiation (λ = 0.15418 nm). The functional groups on the CDs' surfaces were determined by Fourier transform infrared spectroscopy (FT-IR, Thermo Electron, NICOLET 380, Waltham, MA, USA) within the range of 500–4000 $cm^{-1}$. Their optical properties were obtained using a UV–visible spectrophotometer (UV-vis, SHIMADU, UV1800, Kyoto, Japan) and fluorescent spectrometer (LAS-TY-BL1, Suzhou Winray Optoelectronic Technology Co, Ltd., Suzhou, China). The Zeta potentials of the samples were measured by a Zeta potential analyzer (Nano90, Malvern, UK). Their time-resolved fluorescence spectra were measured using a transient fluorescence spectrometer (FLS1000, Edinburgh Instruments, Edinburgh,

UK). An atomic absorption spectrometer was used to analyze the concentration of $Cu^{2+}$ in the real water samples (aa6880, SHIMADU, Kyoto, Japan).

### *2.4. Fluorescence Detection of $Cu^{2+}$*

For the typical fluorescence detection of $Cu^{2+}$, an aliquot of the diluted bf-CDs solution and different amounts of $Cu^{2+}$ were added to a quartz cuvette of 4 mL (Dimensions: 12.5 × 12.5 × 45 mm; Model: 722) to obtain a specific $Cu^{2+}$ concentration. Among them, NaCl, KCl, $Na_2HPO_4$ and $KH_2PO_4$ were added to 10 mM phosphate-buffered saline (PBS), and the pH was adjusted to 7.0. The fluorescence spectrum was measured by the spectrometer at room temperature with an excitation source at 405 nm, which meets the requirements for visible light fluorescence excitation and has the added benefits of safety and common availability. In order to test its selectivity for different ions, its fluorescence response to some reference ions, including $Al^{3+}$, $Mg^{2+}$, $Mn^{2+}$, $Li^{+}$, $K^{+}$, $Sb^{3+}$, $Cd^{2+}$, $Zn^{2+}$, $Hg^{+}$, $Fe^{3+}$, $Cr^{6+}$, was also estimated.

### *2.5. Determination of Fluorescent Quantum Yield*

The quantum yield (QY) of the synthesized CDs was obtained using a relative measurement approach [23]. Quinine sulfate (QY = 54% in sulfuric acid) was selected as the reference dye, and the QY was obtained using

$$\Phi = \Phi' \times \frac{A'}{I'} \times \frac{I}{A} \times \left(\frac{n}{n'}\right)^2 \quad (1)$$

$\Phi$ and $\Phi'$ represent the QY of CDs and quinine sulfate, respectively. I and $I'$ show the integrated emission intensity of the CDs and quinine sulfate, respectively. The values of $n$ and $n'$ are both 1.33. To eliminate the inner filter effect as much as possible, the absorbance was below 0.1 at the excitation wavelength. In addition, the average of five measurements was used to further eliminate experimental errors. The QYs of the CDs and bf-CDs were calculated as 27.1% and 53.6%, respectively.

### *2.6. Real Samples*

To estimate the $Cu^{2+}$ detection ability of our bf-CDs in real samples, three kinds of water were used to replace the DI water in $Cu^{2+}$ detection. The lake water, tap water and sea water were obtained from Sun Moon Lake located at the university's campus, our lab and the Yellow Sea, respectively. To remove suspended particles from the real samples, the three samples were filtered using filter paper (0.22 mm) and centrifuged at 12,000 rpm for 20 min. The $Cu^{2+}$ content in the filtered and centrifuged samples was determined using atomic absorption spectroscopy (AAS).

## 3. Results and Discussion

### *3.1. Characterization of bf-CDs*

A TEM image of CNs obtained using the electrochemical stripping method is shown in Figure S1. The CNs were effectively stripped from the carbon electrode, and their partial enlargement in the image shows the lattice spacing of 0.244 nm, belonging to the (100) facet of $sp^2$ graphitic carbon [24]. The XRD patterns of the CNs on a quartz substrate and corresponding substrate are shown in Figure S2. Their uniform peaks indicate that the characteristic peaks of CNs are not observed, probably due to their small loading amount. Figure 1 illustrates that following the hydrothermal treatment with boric acid, the CNs were effectively converted into CDs and exhibited a small size of less than 10 nm, which could potentially be attributed to thermal agglomeration occurring under the high-temperature and high-pressure conditions within the hydrothermal process. Figure 1b shows a partially

enlarged image of bf-CDs, and a clear lattice structure with a lattice spacing of 0.290 nm can be seen, corresponding to the (020) crystal surface which indicates that carbon dots have been successfully prepared [25,26]. As shown in the inset in panel a, the bf-CDs show a narrow size distribution of 2.3–13.1 nm with an average size of 7.8 nm.

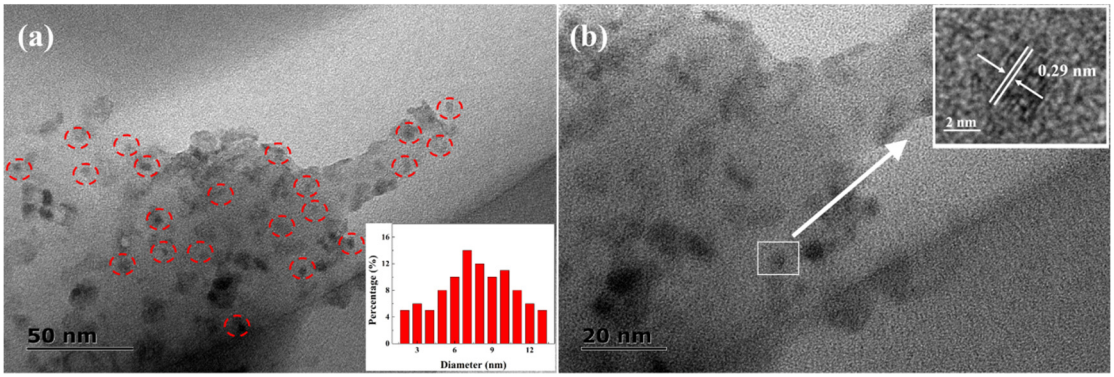



**Figure 1.** (**a**) TEM image of the bf-CDs. (**b**) Partial enlargement image of bf-CDs. Bottom-right inset in panel (**a**) corresponds to the size distribution histogram of CDs. Red circles in panel (**a**) are used to mark the generated CDs. Upper-right inset in panel (**b**) corresponds to an enlarged image of the selected bf-CD.

The FT-IR spectrum was used to estimate the surface functional groups of the CDs. As shown in Figure 2, the characteristic peak in the CDs at 1230 $cm^{-1}$ corresponds to C-N stretching vibrations [27]. The characteristic peaks at 1420, 1600 and 1700 $cm^{-1}$ are assigned to the $COO^-$ groups, the $COO^-$ groups and stretching vibration of C=O, respectively [28–30]. For bf-CDs, the new characteristic peak at 1060 $cm^{-1}$ corresponds to the bonding of B-O-C, which indicates that B was introduced into the bf-CDs [31]. The characteristic peak at 1190 $cm^{-1}$ corresponds to the B-C absorption band, which may be due to the replacement of N in the C-N in the CDs with B [31]. The disappearance of the characteristic peak at 1700 $cm^{-1}$ indicates the disappearance of the functional groups of C=O [32]. In addition, the characteristic peaks at 2260, 2360, and 2510 $cm^{-1}$ may be attributed to the effect of unreacted complete boric acid [33]. Importantly, a new characteristic peak at 3180 $cm^{-1}$ is observed, indicating the formation of -OH groups [34]. The peak intensity at 1420 $cm^{-1}$ is also significantly enhanced, indicating the $COO^-$ groups are introduced to the surface of the bf-CDs. So, the surface of the bf-CDs is surrounded by carboxyl and hydroxyl groups. The hydroxyl and carboxyl groups introduced on the surface of the bf-CDs not only enhance its water solubility, but also display an intense interaction with heavy metal ions, which is applicable to fluorescent detection.

The optical properties of CNs and bf-CDs were studied using UV-vis absorption and fluorescent spectra. For the UV-vis analysis, we focused on the sample's absorption of visible light; therefore, we selected a sample concentration suitable for analyzing absorption intensity in the visible region. As shown in Figure 3a, CNs exhibit almost no visible light absorption and its absorption edge is approximately 320 nm. In contrast, the bf-CDs exhibit evidently enhanced absorption in the whole UV-vis region, and its absorption edge is correspondingly red-shifted to 375 nm, which may be due to the introduction of hydroxyl and carboxyl groups during boric acid functionalization. As shown in Figure 3b, the CNs solution exhibits a weak fluorescent peak at 528 nm due to its weak absorption at 405 nm. In contrast, the bf-CDs show a strong fluorescent peak at 505 nm, corresponding to the band-to-band recombination. Compared to the CNs, the bf-CDs exhibit a blue shift in the fluorescence peak due to the introduction of a large number of functional groups from the modifications, which affects their luminescent properties. In the presence of 90 μM $Cu^{2+}$,

its fluorescence peak is significantly weakened, indicating the strong interaction between the bf-CDs and $Cu^{2+}$.

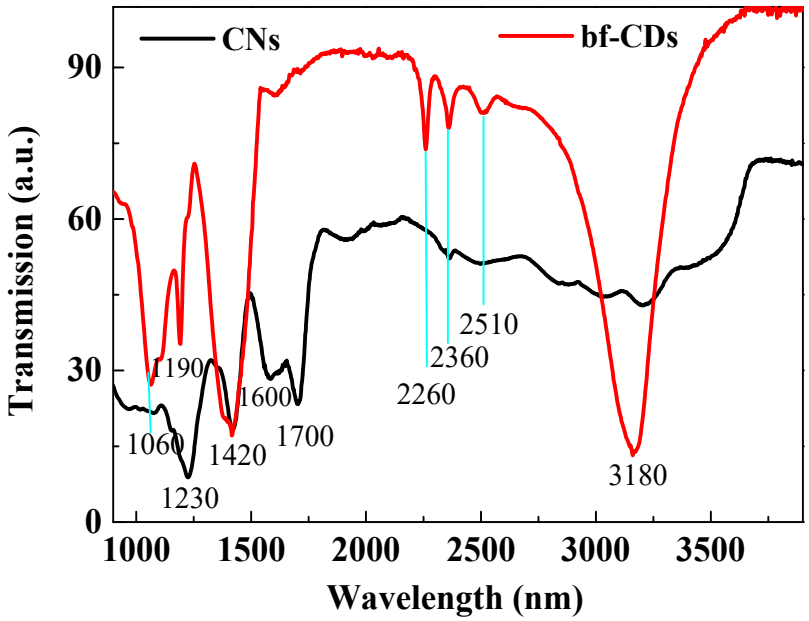



**Figure 2.** FT-IR spectra of CNs and bf-CDs. Where a.u. stands for arbitrary units, which is a unified measurement used to simplify calculations. The blue line in the figure is used to mark the peak position.

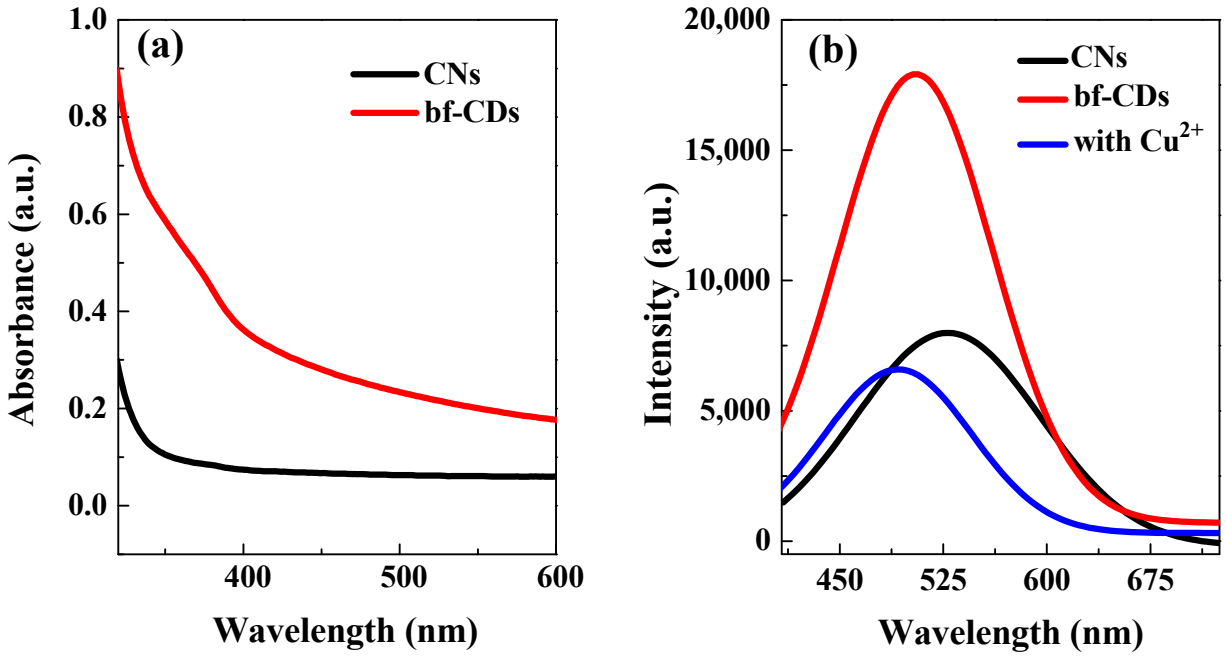



**Figure 3.** (**a**) UV-vis spectra of CNs and bf-CDs. (**b**) Fluorescence peaks of CNs and bf-CDs in the presemce of $Cu^{2+}$ (90 μM) under 405 nm laser irradiation.

### *3.2. Fluorescence Response of bf-CDs to $Cu^{2+}$*

The fluorescence response of the bf-CDs to $Cu^{2+}$ was evaluated, and the results are shown in Figure 4a. When the $Cu^{2+}$ concentration increased, the fluorescence intensity of the bf-CDs gradually weakened. In particular, when the $Cu^{2+}$ concentration increased, the fluorescence peak shifted from 505 nm to 495 nm (Figure 4a), indicating an interaction between the $Cu^{2+}$ and the surface functional groups of the bf-CDs [35,36]. As shown in Figure 4b, there is a good linear relationship ($R^2$ = 0.997) between the peak intensity and the

$Cu^{2+}$ concentration in the range of 0.08–90 μM. The limit of detection (LOD) of the bf-CDs for $Cu^{2+}$ was estimated to be 0.066 μM at a signal-to-noise ratio of 3, and the small error bars show a good repeatability. These results indicate that bf-CDs are able to efficiently detect $Cu^{2+}$.

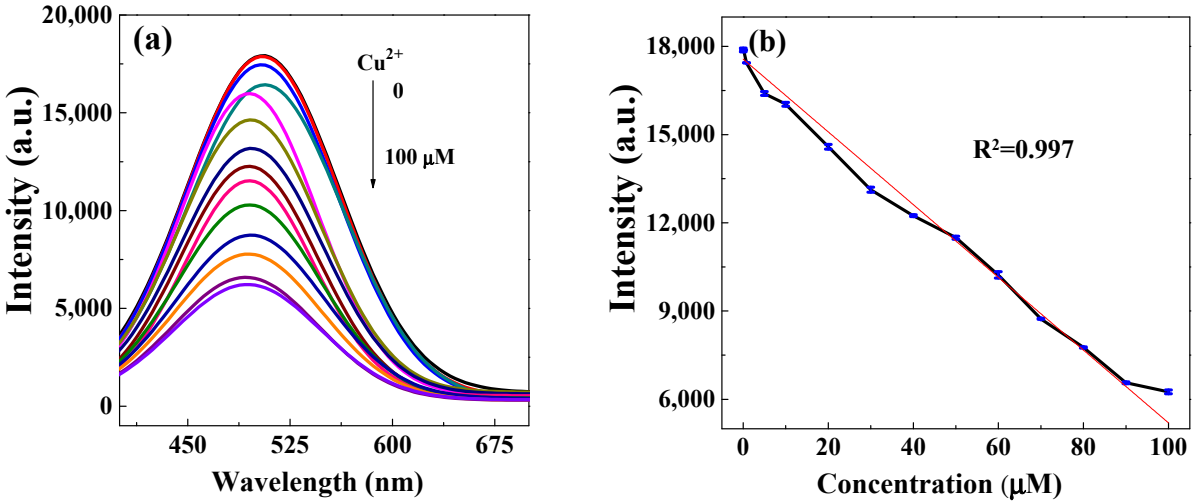



**Figure 4.** (**a**) Fluorescent spectra of bf-CDs in the presence of $Cu^{2+}$ of different concentrations, and represented by different colors of lines. (**b**) Dependence of peak intensity $F_0$ on $Cu^{2+}$ concentrations.

Sensitivity and selectivity are important indicators for fluorescent probes, and the results for the CNs and bf-CDs are shown in Figure 5. First, the fluorescence intensity of the CNs was monitored in the presence of various metal ions (800 μM), as shown in Figure 5a. The CNs exhibited a relatively low sensitivity to all ions (<20%), and their sensitivity to $Cu^{2+}$, $Mn^{2+}$, $Sb^{3+}$, $Cr^{6+}$ and $Li^{+}$ was about equal. In comparison, the bf-CDs exhibited a strong fluorescent response to $Cu^{2+}$ with a sensitivity of up to 65%, and their sensitivity to other ions was below 10%. It is important that there is a small error between the multiple measurements. V is defined as the sensitivity contrast of probes for $Cu^{2+}$ and the strongest reference ion to quantitatively illustrate their selectivity for $Cu^{2+}$. The V of CNs is calculated to be 1.1, so the CDs exhibit a poor selectivity for $Cu^{2+}$. Meanwhile, the value of V reaches 7.0, leading to a high selectivity for $Cu^{2+}$.

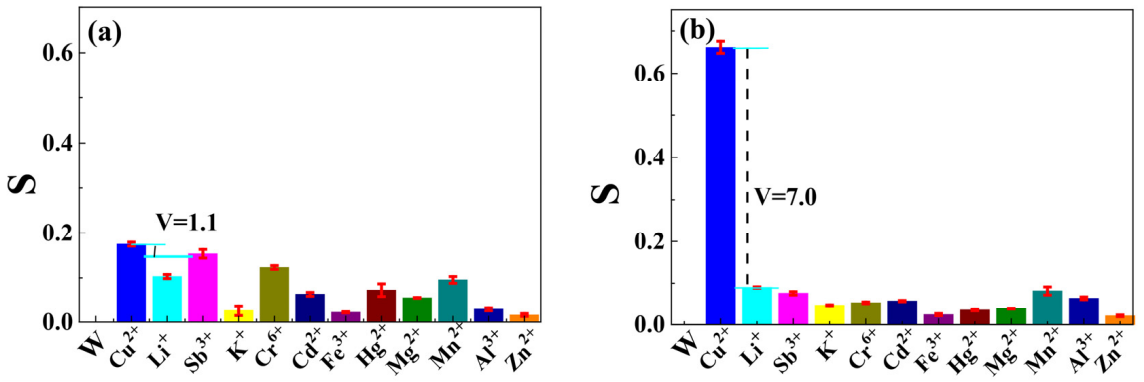



**Figure 5.** (**a**) Fluorescent response of CNs to different ions of 800 μM. (**b**) Fluorescent response of bf-CDs to different ions of 80 μM. S is defined as $S = \frac{F_0 - F}{F_0} * 100\%$; $F_0$ and F are the fluorescence intensity of bare fluorescent probe and that in presence of specific concentrations of ions, respectively. V is defined as $V = \frac{S_{Cu}}{S_r}$; $S_{Cu}$ and $S_r$ are the sensitivity of $Cu^{2+}$ and the strongest reference ion, respectively.

The stability of our bf-CDs was also estimated, as shown in Figure 6. The fluorescence intensity of bf-CDs at different ionic strengths was estimated. As shown in Figure 6a, the

bf-CDs show almost the same fluorescence signal under a NaCl concentration of $10^{-5}$ to 1 M, which indicates their good stability under different ionic strength environment. Figure 6b measures the fluorescence response of the bf-CDs under different pH values. The bf-CDs exhibit the strongest fluorescence response in neutral conditions. The fluorescence response of bf-CDs is clearly reduced under acidic and alkaline conditions, which may due to the protonation of the carboxyl group and the generation of $Cu(OH)_2$ precipitation, respectively [37]. In addition, the dynamics of the bf-CDs probe was also tested, as shown in Figure S3. The fluorescence intensity of the bf-CDs decayed rapidly within 1 min with the addition of $Cu^{2+}$, indicating their real-time detection capability. Meanwhile, the fluorescence intensity of the bf-CDs remains almost unchanged after further irradiation for 40 min, indicating the good stability of the bf-CDs.

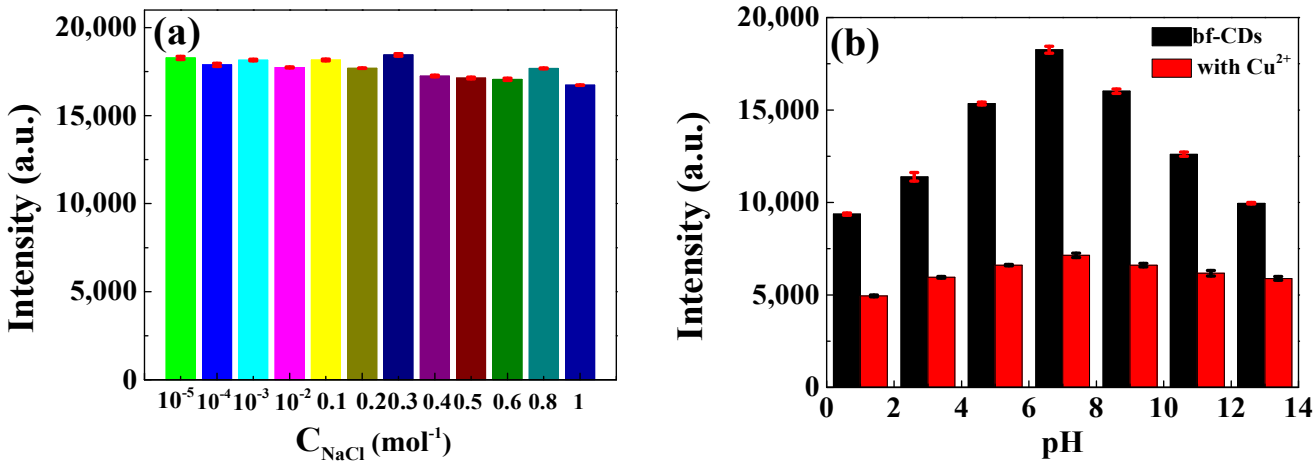



**Figure 6.** (**a**) Fluorescence intensity of bf-CDs in NaCl at a concentration of $10^{-5}$–1M. (**b**) Effect of solution pH on the fluorescence response of bf-CDs.

Then, the response of the bf-CDs to $Cu^{2+}$ was compared with the corresponding results in references [19,20,25,38–42], as shown in Table 1. Doped and functionalized CDs were used to selectively detect $Cu^{2+}$. However, some defects hindered their application, such as a low sensitivity (<43%) [1,5,6,8] or low LOD (>100 nM) [3,5]. Moreover, CDs prepared using the two-step method have also been successfully used for $Cu^{2+}$ detection, but exhibit a low LOD (>300 nM) [41] and low sensitivity (<45%) [42]. In the present work, the bf-CDs can selectively detect $Cu^{2+}$, and have the highest $S_{Cu}/S_r$ of 7.0. In addition, bf-CDs exhibit a wide response interval (0.8–90 μM), relatively high sensitivity (65%) and high LOD (66 nM). The LOD is well below the safety limit of $Cu^{2+}$ in drinking water prescribed by the US Environmental Protection Agency at 1.3 ppm (20 μM).

**Table 1.** Summary of fluorescent probes for $Cu^{2+}$-selective detection.

| Probe. | Synthesis Method | Sensitivity (%) | $S_{Cu}/S_r$ | Response Interval (μM) | LOD (nM) | Ref |
|---|---|---|---|---|---|---|
| N,S/Iy-CDs | Hydrothermal | 16 | 3.6 | 0–0.025 | 45 | [20] |
| P-CDs | Hydrothermal | 23 | 2.6 | 0–0.02 | 1 | [19] |
| N-CDs | Hydrothermal | 30 | 3.1 | 0.1–40 | 90 | [38] |
| ND-CDs | Pyrolysis | 43 | 4.0 | 0.6–30 | 190 | [39] |
| BPEI-CDs | Pyrolysis | 72 | 3.7 | 0.01–1.1 | 6 | [40] |
| CDs | Pyrolysis | 77 | 2.5 | 0.8–80 | 5300 | [25] |
| B, N-CDs | Carbonization and Reflux | 62 | 1.5 | 1–25 | 300 | [41] |
| CDs | Ultrasonic and Reflux | 45 | 2.6 | 0.25–10 | 30 | [42] |
| bf-CDs | Electrochemical and Hydrothermal | 65 | 7.0 | 0.8–90 | 66 | This work |

Note: The $S_{Cu}/S_r$ and S are obtained according to the fluorescence response curve of CDs to different metal ions in above references.

### 3.3. Real Sample Testing

The results of $Cu^{2+}$ detection in the three types of water using AAS are presented in Table 2 and the concentration of $Cu^{2+}$ in the three water samples was less than 0.8 μM, which can be considered negligible. The $Cu^{2+}$ fluorescence detection of bf-CDs in the three types of water was estimated, and the results are listed in Table 2. For the three samples, the measured concentration of $Cu^{2+}$ is very close to the amount added. Meanwhile, the recoveries in the three real sample were between 99.7% and 105.1%, and the values of relative standard deviation (RSD) were below 3.7%. The above results can explain the reliability and accuracy of the bf-CDs for detecting $Cu^{2+}$ in different types of real water.

**Table 2.** Survey of $Cu^{2+}$ in different real water samples.

| Sample | Initial $Cu^{2+}$ (μM) | Added $Cu^{2+}$ (μM) | Measured $Cu^{2+}$ (μM) | Recovery (%) | RSD (%) |
|---|---|---|---|---|---|
| Tap water | 0.37 | 20 | 21.2 | 105.8 | 0.8 |
| | | 90 | 89.7 | 99.7 | 0.6 |
| Lake water | 0.76 | 20 | 21.6 | 107.8 | 1.2 |
| | | 90 | 90.5 | 100.6 | 3.4 |
| Sea water | 0.51 | 20 | 21.4 | 107.1 | 1.5 |
| | | 90 | 89.1 | 99.0 | 3.7 |

Note: The measured concentration is determined based on the linear relationship between the fluorescence intensity of the bf-CDs and the concentration of $Cu^{2+}$ (Figure 4b). Recovery (%) = ($Cu^{2+}$ concentration measured/$Cu^{2+}$ concentration added) × 100%. RSD is relative standard deviation.

### 3.4. Detection Mechanism of bf-CDs for $Cu^{2+}$

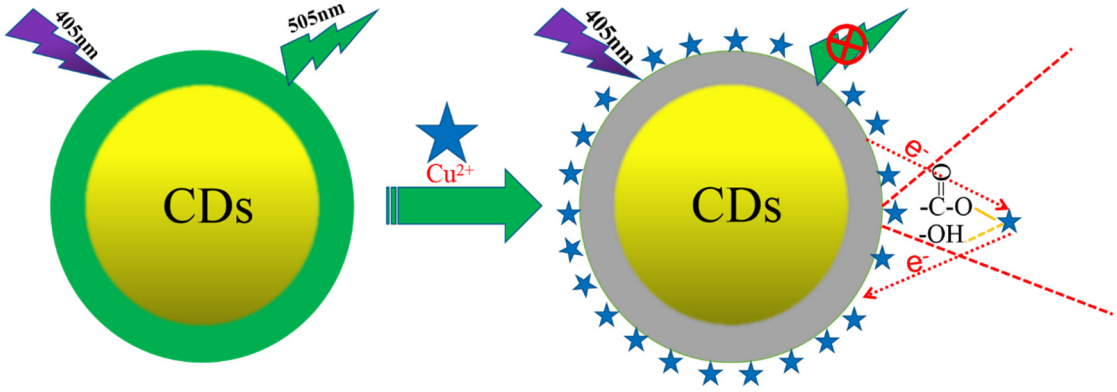
The fluorescence quenching of CDs is typically categorized into static and dynamic types. To investigate the quenching mechanism of bf-CDs in the presence of $Cu^{2+}$, we measured temperature-dependent relationships between the fluorescence intensity of bf-CDs and the concentration of $Cu^{2+}$ ions. As depicted in Figure S4, an increase in the temperature of the CD solution leads to a heightened sensitivity of the bf-CDs to $Cu^{2+}$, suggesting a dynamic quenching mechanism for our CDs [36]. It has been reported that functional groups show a decisive role in the fluorescence response of CDs, which was further explored by FT-IR technology. As shown in Figure S5, when $Cu^{2+}$ is added to the bf-CDs solution, the characteristic peaks at 1420 and 3180 $cm^{-1}$ both exhibit a red shift, indicating that carboxyl and hydroxyl groups can combine with $Cu^{2+}$, determining its fluorescence response to $Cu^{2+}$. The zeta potential of the CDs, as shown in Table S1, is −19.7 mV, while that of bf-CDs is −39.7 mV. The FT-IR results indicate that the surface of the modified bf-CDs has more hydroxyl functional groups. These hydroxyl groups are electronegative, leading to a more negatively charged surface of the bf-CDs, which favors the attraction of $Cu^{2+}$ ions to the surface of the bf-CDs. In addition, $Cu^{2+}$ leads to a decrease in the zeta potential from −39.7 mV to −22.4 mV, indicating the formation of a complex between them.

To further verify the binding of bf-CDs and $Cu^{2+}$, computational calculations were introduced, especially the binding energies of different samples. The Perdew–Burke–Ernzerhof functional within the generalized gradient approximation was used to describe the exchange correlation potential of electrons [43]. Similar to other studies in the literature, the energy cutoff was set to 450 eV, and a vacuum layer (15Å) was used to isolate the correlation between layers. The binding energy of the two bf-CDs/$Cu^{2+}$ systems with the formation of covalent bonds or their physical contact is calculated using Equation (1) [43]:

$$E_{binding\ energy} = E_{total}\left(bf\text{-}CDs/Cu^{2+}\right) - E_{total}(bf\text{-}CDs) - E_{total}\left(Cu^{2+}\right) \quad (2)$$

Due to the formation of covalent bonds, the binding energy of bf-CDs/$Cu^{2+}$ is reduced by 0.57 eV, indicating that covalent bonds are more inclined to form between bf-CDs and $Cu^{2+}$. In addition, the binding energy of the bf-CDs/$Cu^{2+}$ systems is much lower than that of the CDs/$Cu^{2+}$ systems, so the introduction of carboxyl and hydroxyl groups on the surface of bf-CDs can enhance its binding with $Cu^{2+}$, and they tend to exhibit covalent bonding, which corresponds to its improved sensitivity. To analyze the charge carrier dynamics of the CNs/$Cu^{2+}$ and bf-CDs/$Cu^{2+}$ systems, their time-resolved fluorescence spectra were measured, and the results are shown in Figure S6 and Table S2. The obtained decay curves are fitted with the bi-exponential decay function; among them, the fast decay process ($\tau_1$) is attributed to exciton trapping due to the surface defects of the CNs and bf-CDs, and the fast decay process ($\tau_2$) can be traced to exciton recombination at interface defects. Compared with the CNs, the bf-CDs show a shorter $\tau_2$, indicating that the introduction of covalent bonds can inhibit the interface carrier recombination, thereby improving the detection performance.

The detection mechanism for the detection of $Cu^{2+}$ by bf-CDs is shown in Scheme 1. In detail, when the bf-CDs were free, they showed strong fluorescence signals. With the addition of $Cu^{2+}$ to the bf-CD solution, the complexation between $Cu^{2+}$ and functional groups (hydroxyl and carboxyl groups) of bf-CDs resulted in the splitting of the d orbital of $Cu^{2+}$ [44]. So, electrons in the excited state of bf-CDs have a chance to transfer to the d orbital of $Cu^{2+}$, which leads to nonradiative electron/hole recombination and results in fluorescence quenching.




**Scheme 1.** Schematic diagram of fluorescence signal response of bf-CDs to $Cu^{2+}$.The five-pointed star represents the added $Cu^{2+}$, and the $e^-$ represents the photogenerated electron.

$Cu^{2+}$ can bind tightly to the carboxyl and hydroxyl groups on the surface of bf-CDs, and Figure 2 clearly illustrates that abundant hydroxyl and carboxyl groups were introduced to the surface of the bf-CDs. So, the bf-CDs exhibit an improved selectivity to $Cu^{2+}$ [44]. The standard form potential ($E_0$) of $Mn^+/M$ is more positive than the hole potential on bf-CDs and more negative than the electrons on bf-CDs. Therefore, electrons can easily transfer from bf-CDs to $Cu^{2+}$ [45]. In addition, the highest absorption affinity of $Cu^{2+}$ to bf-CDs may also be the reason for the high selectivity of bf-CDs [4].

## 4. Conclusions

In summary, a simple and efficient electrochemical method was used to synthesize CDs, which was followed by the hydrothermal method to prepare bf-CDs. The bf-CDs showed a narrow size distribution (2.3–13.1 nm) and were modified with abundant functional groups such as carboxyl and hydroxyl groups. The bf-CDs show high selectivity and sensitivity of 65% to $Cu^{2+}$. However, the bf-CDs exhibit short response time of less than 1 min and a high LOD of 0.066 μM. The mechanism of the $Cu^{2+}$-induced fluorescence quenching of bf-CDs

is a non-radiative electron transfer processes. The improved selectivity of bf-CDs for $Cu^{2+}$ is mainly due to the introduction of specific functional groups (hydroxyl and carboxyl groups) onto the surface of the bf-CDs. In addition, the sensor was successfully applied in the detection of $Cu^{2+}$ in three water samples. However, this work lacks an analysis of the electron transfer behavior at the interface between carbon dots and copper ions. In future work, we plan to analyze the electron transfer behavior at the interface through theoretical simulation calculations to further elucidate the interaction mechanism between CDs and $Cu^{2+}$.

**Supplementary Materials:** The following supporting information can be downloaded at: https://www.mdpi.com/article/10.3390/cryst15030205/s1, Figure S1: (a) TEM image of the CNs. (b) Partial enlargement image of CNs. Figure S2: XRD patterns of the CNs on quartz glass substrate and the glass substrate. Figure S3: Fluorescence intensity of bf-CDs as a function of reaction time. Figure S4: Temperature dependent curves between fluorescence intensity of bf-CDs and ions concentration. Figure S5: FT-IR spectra of bf-CDs and that in present of $Cu^{2+}$. Figure S6: Time-resolved photoluminescence decay curves of CNs and bf-CDs; Table S1: Zeta potential of bf-CDs, $Cu^{2+}$ and bf-CDs/$Cu^{2+}$ dispersed in DI water. Table S2: Fitting decay parameters of the fluorescence spectra of CNs and bf-CDs.

**Author Contributions:** Conceptualization, X.Z., H.Z., S.R. and Y.Z.; methodology, X.Z., H.J., L.S. and X.G.; software, Y.S., X.Z. and Y.Z.; validation, S.R., L.S. and X.G.; formal analysis, X.Z., H.Z. and X.G.; investigation, H.J., L.S. and Y.S.; resources, Q.L., S.R. and Y.Z.; data curation, X.Z. and H.J.; writing—original draft preparation, X.Z., H.J. and H.Z.; writing—review and editing, Y.Z. and S.R.; supervision, Q.L. and X.G.; funding acquisition, X.Z. and Y.Z. All authors have read and agreed to the published version of the manuscript.

**Funding:** This work was supported by the Natural Science Foundation of Shandong Province (Grant No. ZR2024QB387), the Foundation of Yantai Vocational College (Grant No. 2023XBYB009) and the Natural Science Foundation of Shandong Province (Grant No. ZR2024QB388).

**Data Availability Statement:** The original contributions presented in this study are included in the article. Further inquiries can be directed to the corresponding authors.

**Conflicts of Interest:** The authors declare no conflicts of interest.

## References

1. Zietz, B.P.; de Vergara, J.D.; Dunkelberg, H. Copper concentrations in tap water and possible effects on infant's health-results of a study in lower saxony, Germany. *Environ Res.* **2003**, *92*, 129–138. [CrossRef] [PubMed]
2. Yang, S.; Guo, W.; Sun, X. Electrostatic association complex of a polymer capped CdTe(S) quantum dot and a small molecule dye as a robust ratiometric fluorescence probe of copper ions. *Dye. Pigment.* **2018**, *158*, 114–120. [CrossRef]
3. Yao, J.; Zhang, K.; Zhu, H.; Ma, F.; Sun, M.; Yu, H.; Sun, J.; Wang, S. Efficient ratiometric fluorescence probe based on dual-emission quantum dots hybrid for on-site determination of copper ions. *Anal. Chem.* **2013**, *85*, 6461–6468. [CrossRef] [PubMed]
4. Tan, X.; Romainor, A.N.B.; Chin, S.; Ng, S.M. Carbon dots production via pyrolysis of sago waste as potential probe for metal ions sensing. *J. Anal. Appl. Pyrolysis* **2014**, *105*, 157–165. [CrossRef]
5. Bao, Y.; Zhang, H.; Wu, X.; Yan, R.; Wang, Z.; Guo, C.; Jin, Y. Dual-responsive Cu(I) and Cu(II) co-doped carbon dots for synergistic chemodynamic-photothermal antitumor therapy. *ACS Appl. Nano Mater.* **2023**, *6*, 14410–14420. [CrossRef]
6. Gao, T.; Deng, P.; Guo, S.; Zhang, J.; Cai, Y.; Hu, Z.; Cai, Q.; Liu, Y. Selective and sensitive detection of $Cu^{+}$ in living cells based on chelator modified carbon dots. *Adv. Opt. Mater.* **2024**, *12*, 2400458. [CrossRef]
7. Cui, Y.; Yang, D.; Li, Q.; Peng, Z.; Zhong, Z.; Song, Y.; Han, Q.; Yang, Y. Cu, Zn, I-doped carbon dots with boosted triple antioxidant nanozyme activity for treatment of DSS-induced colitis. *ACS Appl. Mater. Interfaces* **2024**, *16*, 32619–32632. [CrossRef] [PubMed]
8. Mai, X.; Bui, T.; Tran, D.; Mai, V.; Duong, N.H.; Nguyen, V.H. One-pot synthesis of homogeneous carbon quantum dots/aluminum hydroxide composite and its application in Cu(II) detection. *Carbon Lett.* **2024**, *34*, 603–609. [CrossRef]

9. El-Azazy, M.; AlReyashi, O.A.; Al-Saad, O.K.; Al-Hashimi, O.N.; Mohammad, O.; Al-Ghouti, A.; Mohamed, O.; Shibl, F.; Alahzm, O.A.; El-Shafie, A.S. Mandarin peels-derived carbon dots: A multifaceted fluorescent probe for Cu(II) detection in tap and drinking water samples. *Nanomaterials* **2024**, *14*, 1666. [CrossRef]
10. Xiong, Y.; Chen, M.; Mao, Z.; Deng, Y.; He, J.; Mu, H.; Li, P.; Zou, W.; Zhao, Q. Synthesis of up-conversion fluorescence N-doped carbon dots with high selectivity and sensitivity for detection of $Cu^{2+}$ ions. *Crystals* **2023**, *13*, 812. [CrossRef]
11. Liu, S.; Tian, J.; Wang, L.; Zhang, Y.; Qin, X.; Luo, Y.; Asiri, A.W.; Al-Youbi, A.O.; Sun, X. Hydrothermal treatment of grass: A low-cost, green route to nitrogen-doped, carbon-rich, photoluminescent polymer nanodots as an effective fluorescent sensing platform for label-free detection of Cu(II) ions. *Adv. Mater.* **2012**, *24*, 2037–2041. [CrossRef]
12. Zhang, Z.; Hao, J.; Zhang, J.; Zhanga, B.; Tang, J. Protein as the source for synthesizing fluorescent carbon dots by a one-pot hydrothermal route. *RSC Adv.* **2012**, *2*, 8599–8601. [CrossRef]
13. Zhai, X.; Zhang, P.; Liu, C.; Bai, T.; Li, W.; Daic, A.; Liu, W. Highly luminescent carbon nanodots by microwave-assisted pyrolysis. *Chem. Commun.* **2012**, *48*, 7955–7957. [CrossRef]
14. Wei, T.; Ni, H.; Ren, X.; Zhou, W.; Gao, H.; Hu, S. Fabrication of nitrogen-doped carbon dots biomass composite hydrogel for adsorption of Cu (II) in wastewater or soil and DFT simulation for adsorption mechanism. *Chemosphere* **2024**, *361*, 142432. [CrossRef] [PubMed]
15. Liu, H.; Ye, T.; Mao, C. Fluorescent carbon nanoparticles derived from candle soot. *Angew. Chem. Int. Ed.* **2007**, *46*, 6473–6475. [CrossRef] [PubMed]
16. Wang, Q.; Liu, X.; Zhang, L.; Lv, Y. Microwave-assisted synthesis of carbon nanodots through an eggshell membrane and their fluorescent application. *Analyst* **2012**, *137*, 5392–5397. [CrossRef] [PubMed]
17. Zheng, M.; Liu, S.; Li, J.; Qu, D.; Zhao, H.; Guan, X.; Hu, X.; Xie, Z.; Jing, X.; Sun, Z. Integrating oxaliplatin with highly luminescent carbon dots: An unprecedented theranostic agent for personalized medicine. *Adv. Mater.* **2014**, *26*, 3554–3560. [CrossRef]
18. Chen, J.; Li, Y.; Lv, K.; Zhong, W.; Wang, H.; Wu, Z.; Yi, P.; Jiang, J. Cyclam-functionalized carbon dots sensor for sensitive and selective detection of copper(II) ion and sulfide anion in aqueous media and its imaging in live cells. *Sens. Actuators B* **2016**, *224*, 298–306. [CrossRef]
19. Yang, F.; He, X.; Wang, C.; Cao, Y.; Li, Y.; Yan, L.; Liu, M.; Lv, M.; Yang, Y.; Zhao, X.; et al. Controllable and eco-friendly synthesis of P-riched carbon quantum dots and its application for copper (II) ion sensing. *Appl. Surf. Sci.* **2018**, *448*, 589–598. [CrossRef]
20. Radhakrishnan, K.; ORCID, P.P.; Marieeswaran, M. A green synthetic route for the surface-passivation of carbon dots as an effective multifunctional fluorescent sensor for the recognition and detection of toxic metal ions from aqueous solution. *Anal. Methods* **2019**, *11*, 490–506. [CrossRef]
21. Roshni, V.; Misra, S.; Santra, M.K.; Ottoor, D. One pot green synthesis of C-dots from groundnuts and its application as Cr (VI) sensor and in vitro bioimaging agent. *J. Photochem. Photobiol. A Chem.* **2019**, *373*, 28–36.
22. Ming, H.; Ma, Z.; Liu, Y.; Pan, K.; Yu, H.; Wang, F.; Kang, Z. Large scale electrochemical synthesis of high quality carbon nanodots and their photocatalytic property. *Dalton Trans.* **2012**, *41*, 9526. [CrossRef] [PubMed]
23. Zhang, Y.; Fang, X.; Zhao, H.; Li, Z. A highly sensitive and selective detection of Cr(VI) and ascorbic acid based on nitrogen-doped carbon dots. *Talanta* **2018**, *181*, 318–325. [CrossRef] [PubMed]
24. Liu, Y.; Liu, Y.; Park, S.; Zhang, Y.; Kim, T.; Chae, S.; Park, M.; Kim, H.K. One-step synthesis of robust nitrogen-doped carbon dots: Acid-evoked fluorescence enhancement and their application in $Fe^{3+}$ detection. *J. Mater. Chem. A* **2015**, *3*, 17747. [CrossRef]
25. Zheng, X.; Liu, W.; Gai, Q.; Tian, Z.; Ren, S. A carbon-dot-based fluorescent probe for the sensitive and selective detection of copper(II) ions. *ChemistrySelect* **2019**, *4*, 2392–2397. [CrossRef]
26. Guo, L.; Ge, J.; Liu, W.; Niu, G.; Jia, Q.; Wang, H.; Wang, P. Tunable multicolor carbon dots prepared from well-defined polythiophene derivatives and their emission mechanism. *Nanoscale* **2016**, *8*, 729–734. [CrossRef]
27. Wang, Y.; Bai, X.; Pan, C.; He, J.; Zhu, Y. Enhancement of photocatalytic activity of $Bi_2WO_6$ hybridized with graphite-like $C_3N_4$. *J. Mater. Chem.* **2012**, *22*, 11568. [CrossRef]
28. Wang, S.; Niu, H.; He, S.; Cai, Y. One-step fabrication of high quantum yield sulfur- and nitrogen-doped carbon dots for sensitive and selective detection of Cr(VI). *RSC Adv.* **2016**, *6*, 107717. [CrossRef]
29. Lu, W.; Qin, X.; Liu, S.; Chang, G.; Zhang, Y.; Luo, Y.; Asiri, A.M.; Al-Youbi, A.O.; Sun, X. Economical, green synthesis of fluorescent carbon nanoparticles and their use as probes for sensitive and selective detection of mercury(II) ions. *Anal. Chem.* **2012**, *84*, 5351–5357. [CrossRef] [PubMed]
30. Wang, B.; Song, A.; Feng, L.; Ruan, H.; Li, H.; Dong, S.; Hao, J. Tunable amphiphilicity and multifunctional applications of ionic-liquid-modified carbon quantum dots. *ACS Appl. Mater. Interfaces* **2015**, *7*, 6919–6925. [CrossRef] [PubMed]
31. Sadhanala, H.K.; Nanda, K.K. Boron-doped carbon nanoparticles: Size-independent color tunability from red to blue and bioimaging applications. *Carbon* **2016**, *96*, 166–173. [CrossRef]
32. Yakusheva, A.; Aly-Eldeen, M.; Gusev, A.; Zakharova, O.; Kuznetsov, D. Cyan fluorescent carbon quantum dots with amino derivatives for the visual detection of copper (II) cations in sea water. *Nanomaterials* **2023**, *13*, 1004. [CrossRef]

33. Han, Y.; Tang, D.; Yang, Y.; Li, C.; Kong, W.; Huang, H.; Liu, Y.; Kang, Z. Non-metal single/dual doped carbon quantum dots: A general flame synthetic method and electro-catalytic properties. *Nanoscale* **2015**, *7*, 5955. [CrossRef]
34. Liu, S.; Cui, J.; Huang, J.; Tian, B.; Jia, F.; Wang, G. Facile one-pot synthesis of highly fluorescent nitrogen-doped carbon dots by mild hydrothermal method and their applications in detection of Cr(VI) ions. *Spectrochim. Acta Part A Mol. Biomol. Spectrosc.* **2019**, *206*, 65–71. [CrossRef]
35. Wang, Y.; Wu, W.; Wu, M.; Sun, H.; Xie, H.; Hu, C.; Wu, X.; Qiu, J. Yellow-visual fluorescent carbon quantum dots from petroleum coke for the efficient detection of $Cu^{2+}$ ions. *New Carbon Mater.* **2015**, *30*, 550–559. [CrossRef]
36. Zheng, X.; Ren, S.; Wang, L.; Gai, Q.; Dong, Q.; Liu, W. Controllable functionalization of carbon dots as fluorescent sensors for independent Cr(VI), Fe(III) and Cu(II) ions detection. *J. Photochem. Photobiol. A Chem.* **2021**, *417*, 113359. [CrossRef]
37. Vedamalai, M.; Periasamy, A.P.; Wang, C.; Tseng, Y.; Ho, L.; Shiha, S.; Chang, S. Carbon nanodots prepared from*α*-phenylenediamine for sensing of $Cu^{2+}$ ions in cells. *Nanoscale* **2014**, *6*, 13119. [CrossRef] [PubMed]
38. Liao, S.; Huang, X.; Yang, H.; Chen, X. Nitrogen-doped carbon quantum dots as a fluorescent probe to detect copper ions, glutathione, and intracellular pH. *Anal. Bioanal. Chem.* **2018**, *410*, 7701–7710. [CrossRef] [PubMed]
39. Zhao, L.; Li, H.; Xu, Y.; Liu, H.; Zhou, T.; Huang, N.; Li, Y.; Ding, D. Selective detection of copper ion in complex real samples based on nitrogen-doped carbon quantum dots. *Anal. Bioanal. Chem.* **2018**, *410*, 4301–4309. [CrossRef] [PubMed]
40. Dong, Y.; Wang, R.; Li, G.; Chen, C.; Chi, Y.; Chen, G. Polyamine-functionalized carbon quantum dots as fluorescent probes for selective and sensitive detection of copper ions. *Anal. Chem.* **2012**, *84*, 6220–6224. [CrossRef] [PubMed]
41. Rong, M.; Zhang, K.; Wang, Y.; Chen, X. The synthesis of B, N-carbon dots by a combustion method and the application of fluorescence detection for $Cu^{2+}$. *Chin. Chem. Lett.* **2017**, *28*, 1119–1124. [CrossRef]
42. Liu, W. A highly selective and sensitive electrochemical sensor based on ion-imprinted magnetic carbon nanospheres for Cu(II) detection. *New Carbon Mater.* **2015**, *30*, 550–559.
43. Zheng, X.; Wang, Y.; Ren, S.; Gai, Q.; Liu, W.; Dong, Q. Construction of interfacial P-Ni bonding for enhanced hydrogen evolution performance of P-doped $C_3N_4$/Ni photocatalysts. *ACS Appl. Energy Mater.* **2022**, *5*, 5756–5765. [CrossRef]
44. Wang, J.; Sheng, R.L.; Zhang, H.; Wang, N.; Zhang, Z.; Huang, C. Highly fluorescent carbon dots as selective and visual probes for sensing copper ions in living cells via an electron transfer process. *Biosens. Bioelectron.* **2017**, *97*, 157–163. [CrossRef] [PubMed]
45. Zhu, A.; Qu, Q.; Shao, X.; Kong, B.; Tian, Y. Carbon-dot-based dual-emission nanohybrid produces a ratiometric fluorescent sensor for in vivo imaging of cellular copper ions. *Angew. Chem. Int. Ed.* **2012**, *51*, 7185–7189. [CrossRef] [PubMed]


**Disclaimer/Publisher's Note:** The statements, opinions and data contained in all publications are solely those of the individual author(s) and contributor(s) and not of MDPI and/or the editor(s). MDPI and/or the editor(s) disclaim responsibility for any injury to people or property resulting from any ideas, methods, instructions or products referred to in the content.